Soils and Foundations 2015;55(5):985–1000

HOSTED BY

ELSEVIER

CrossMark

The Japanese Geotechnical Society

Soils and Foundations

www.sciencedirect.com
journal homepage: www.elsevier.com/locate/sandf

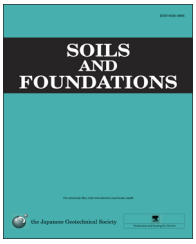

Multi-point shaking table test of the free field under non-uniform earthquake excitation

Xiao Yan[a], Haitao Yu[b,c,*], Yong Yuan[d], Juyun Yuan[b]

[a]Department of Geotechnical Engineering, Tongji University, 1239, Siping Road, Shanghai 200092, China
[b]Key Laboratory of Geotechnical and Underground Engineering of Ministry of Education, Tongji University, 1239 Siping Road, Shanghai 200092, China
[c]Department of Civil Engineering, Shanghai Jiaotong University, 800 Dongchuan Road, Shanghai 200030, China
[d]State Key Laboratory of Disaster Reduction in Civil Engineering, Tongji University, 1239 Siping Road, Shanghai 200092, China

Received 30 June 2014; received in revised form 3 August 2015; accepted 3 September 2015

Abstract

A series of shaking table tests of model field were conducted using four shaking tables. Details of experimental setup are first presented with particular focus on design of the similitude ratio, the 40-m-long model boxes, and the synthetic model soil. The experiments were conducted in two phases: Phase 1 is shaking table test of the model boxes without soil; while Phase 2 is the model field shaking table test. Test results including response acceleration and its spectrum are discussed. The comparisons show that non-uniform excitation in different wave form, peak acceleration, vibration direction and wave propagation direction may lead to different dynamic response. The wave passage effects caused by earthquake should be considered in study of seismic response of long-shape field.

Keywords: Model ground; Multi-point shaking table; Non-uniform excitation; Earthquake

1. Introduction

The Hong Kong–Zhuhai–Macau (HZM) Bridge (under construction) is located on the Pearl River Delta district in south China. It connects three world famous cities in south China. The east direction of HZM Bridge connects Hong Kong, while Zhuhai and Macau are connected at the westward, as shown in Fig. 1. The HZM Bridge consists of three different engineering components: a series of cross-sea bridges, double man-made islands and an ultra-long immersed tunnel (5670 m long). The key point of these mega structures is the immersed tunnel.

Given the experience accumulated from past performance of buried structures during strong seismic motions, tunnels are particularly sensitive to earthquake damage due to their shallow burial depth and slender shape (Hashash et al., 2001). The issue is even difficult by the fact that immersed tunnels are typically surrounded by soft soils with different physical and mechanical properties. Such complicated geology is associated with complex propagation of earthquake-induced motions, which in turn will induce complex tunnel deformations. Other factors such as soil–structure interaction, large hydrostatic pressures and saturated soils add to the complexity of the problem (Kasper et al., 2008). Thus, finding out dynamic characteristics of soil ground is necessary. However, there are no reliable analytical or empirical tools for such

*Corresponding author at: Key Laboratory of Geotechnical and Underground Engineering of Ministry of Education, Tongji University, Shanghai, PR China. Tel.: +86 21 65984573.
E-mail addresses: yuhaitao@tongji.edu.cn (H. Yu), yuany@tongji.edu.cn (J. Yuan).
Peer review under responsibility of The Japanese Geotechnical Society.

http://dx.doi.org/10.1016/j.sandf.2015.09.031

analysis, and appropriate mechanical parameters are hard to be chosen for numerical model. Therefore, large-scale shaking table tests should better be employed to study the seismic performance of the vast tunnel field.

Generally, ground field where immersed tunnel locates tends to be man-made trench of high slope and long extension. In practice, it is of particular interest to predict the dynamic response of a man-made slope under seismic loadings (Newmark, 1965; Gazetas, 1987; Ling, et al., 1997; Hong, et al., 2005). In order to study dynamic behavior of slope associated with earthquake, approach of physical model test, such as centrifuge model test and shaking table test, was utilized. Kutter (1983) conducted centrifuge test with clay soil and found that the displacement predicted with strain softening would better coincide with the test results. Through a series of dynamic centrifuge tests, Brennan et al. (2005) evaluated shear modulus and damping ratio of soil. However, a major problem of centrifuge model test is that there may have scaling effect due to the difficulty of scaling the instrumentation properly.

Shaking table test is another important approach to study seismic response of soil slope. Lo Grasso et al. (2004) investigated the performance of reinforced slope through a number of shaking table tests. It was concluded from the study that reducing the spacing of reinforcement near the top of the model is beneficial for the stability of the slope. Lin and Wang (2006) conducted shaking table test to identify the initiate status of landslide movement from the acceleration time-history curves based on nonlinear behaviour of slope soil. In order to understand the influences of peak horizontal ground accelerations and wave frequencies on seismic displacement of slope, Huang et al. (2011) carried out a shaking table test on reinforced model slope. Long-shape structure is always considered to sustain non-uniform loadings due to earthquake. Then, multi-point shaking table test is needed to investigate seismic response of long structure and its field. Chen et al. (2010) conducted a series of shaking table tests of utility tunnel model using two isolate shaking tables. Test results indicated that the effect of spatial distribution of earthquake excitation should be considered.

This paper presents a series of shaking table tests of scaled free field using four shaking tables. In particular, the design of this test focuses on the similitude ratio, model boxes and synthetic soil. The tests were conducted in two phases: Phase 1 is shaking table test of model boxes without soil; while Phase 2 is model field test. Test results of different excitation cases were compared.

2. Set-up of test

2.1. Shaking table system

The tests were performed in the State Key Laboratory of Disaster Reduction in Civil Engineering in Tongji University.

Fig. 1. Geographic position of HZM Bridge (Fang, et al., 2011).

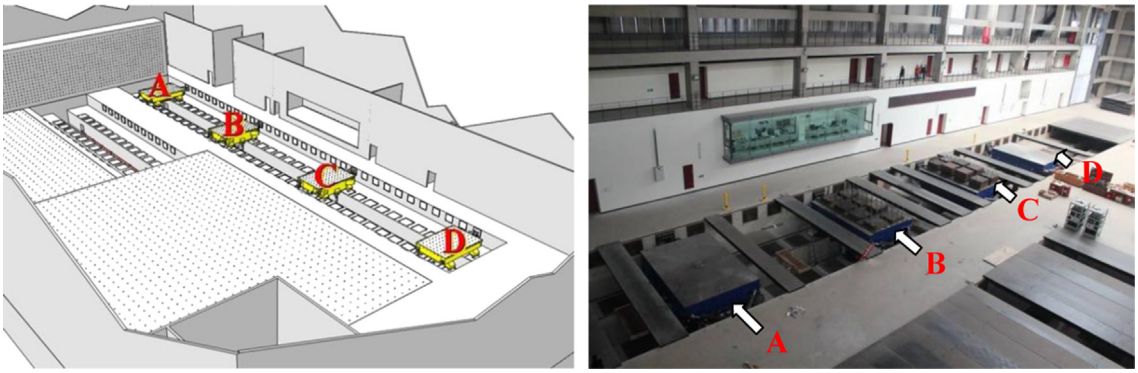

Fig. 2. The multiple shake table testing system.

The multi-function shaking table system is composed of two main tables with 700 kN payload each, two other tables with 300 kN payload each, and a 70-m long test trench, as shown in Fig. 2. All four tables are moveable along three-degrees-of freedom (transversal, longitudinal and rotational) in the test trench and work as a large linear shake table array. The dimension of each table is 4 m × 6 m (4 m is along the longitudinal direction of test trench, while 6 m is perpendicular to the trench). The maximum acceleration of each shaking table is ± 1.5 g, where g is the acceleration due to gravity in m/s^2.

2.2. Design of similitude relation

In design of shaking table test, the issue of similitude is always encountered firstly. The similitude relations in this paper were obtained in basis of the Buckingham-π theorem, which was widely used for design of shaking table tests by other researchers. Based on the theory, Meymand (1998) designed the scale-model clay, which was used in the shaking table test of soil–pile–structure model. Moss and Crosariol (2013) developed model soil and model tunnel for shaking table test following the similitude theory. Iai (1989) derived a similitude relation for a 1 g shaking table test of saturated soil–structure–fluid model.

In the basis of the Buckingham-π theorem, dimensional analysis (Meymand, 1998) was developed to find out the similitude relation of critical physical parameters. Assuming the stress–strain relation of the soil could be formulated by hyperbolic model as

$$\sigma = \frac{\varepsilon}{a + b\varepsilon} \tag{1}$$

where σ and ε are stress and strain, respectively, and the parameters a and b are constant quantities. Then Eq. (1) can be formed as

$$\frac{\sigma}{E} = \varepsilon \frac{1}{aE + b\sigma} \tag{2}$$

where E is Young's modulus. According to theorem of dimensional analysis and similitude, similitude ratios of physical quantities with same dimension could be regarded as equivalent. For Eq. (2), the dimension of either stress σ or Young's modulus E is N/m^2. The dimension of a and b is m^2/N, and strain ε is dimensionless variable which is always expressed as 1. It can be deduced that the dimension of each side of Eq. (2) is the same, and the similitude ratio of stress is equal to Young's modulus, which can be expressed as

$$\begin{cases} \dfrac{S_\sigma}{S_E} = 1 \\ S_\varepsilon = 1 \end{cases} \tag{3}$$

where S_σ, S_E and S_ε stand for similitude ratio for stress, Young's modulus and strain, respectively. It is commonly concluded from test results that the shear modulus G of sandy soil is proportional to the square root of confining stress σ (Iwasaki, et al., 1978). However, dimensional analysis only focuses on dimensions of physical quantities instead of physical relations, that is physical quantities with same dimension earn the same similitude ratio. Then, it makes sense that Eq. (3) is different from the common physical relation.

Second, similitudes for soil parameters, such as geometry, density and shear modulus, are critical in shaking table test. The similitude ratio for the shear modulus is found from the classic dynamic equation, i.e.,

$$\rho \frac{\partial^2 u}{\partial t^2} = (\lambda + G)\frac{\partial \varepsilon}{\partial x} + G\nabla^2 u \tag{4}$$

where ρ, u and t is density, displacement and time, respectively, while λ, G and x is the Lame's constant, shear modulus and the position coordinate, respectively. Then, Eq. (4) can be expressed as

$$\frac{\rho \frac{\partial^2 u}{\partial t^2} - \lambda \frac{\partial \varepsilon}{\partial x}}{\frac{\partial \varepsilon}{\partial x} + \nabla^2 u} = G \tag{5}$$

The dimension of ρ is kg m^{-3}, $\partial^2 u/\partial t^2$ is m s$-^2$, λ is kg m^{-1} s^{-1}, $\partial\varepsilon/\partial x$ is m^{-1}, $\nabla^2 u$ is m^{-1} and G is kg m^{-1} s^{-1}. Same dimension is observed at both sides of the equation. Similitude relation could be expressed by dimensional analysis, i.e. the similitude ratio for ρ is S_ρ, the similitude ratio for $\partial^2 u/\partial t^2$ is S_a, the similitude ratio for $\partial\varepsilon/\partial x + \nabla^2 u$ is S_l^{-1}, and the similitude ratio for G is S_G. In addition, $(\lambda)\partial\varepsilon/\partial x$ is negligible in dimensional analysis due to the same dimension as $(\rho)\partial^2 u/\partial t^2$. Hence, the similitude ratio for dynamic shear modulus could be deduced as

$$\frac{G_d^m}{G_d^p} = S_{G_d} = S_l \cdot S_\rho \cdot S_a \tag{6}$$

where G_d^m and G_d^p is dynamic shear modulus of model and prototype, respectively.

Similitude relations for other parameters were derived in similar method. For example, the relation of density, volume and mass is $m=\rho v$. Dimension of the mass, density and volume is kg, kg m^{-3} and m^3, respectively. Then, the similitude ratio for mass can be obtained as

$$S_m = S_\rho \cdot S_l^3 \tag{7}$$

Similarly, the shear wave velocity v_s is expressed with the density ρ and the shear modulus G as:

$$v_s = \sqrt{\frac{G}{\rho}} \tag{8}$$

and thus similitude relation can be expressed as

$$S_v = S_G^{1/2} \cdot S_\rho^{-1/2} \tag{9}$$

Also, the velocity v is related to distance l and time t, $v=l/t$. Then, similitude ratio for time is obtained as

$$S_t = S_l \cdot S_v^{-1} = S_l \cdot S_\rho^{1/2} \cdot S_G^{-1/2} \tag{10}$$

And the similitude ratio for frequency can be deduced as

$$S_\omega = S_t^{-1} = S_l^{-1} \cdot S_\rho^{-1/2} \cdot S_G^{1/2} \tag{11}$$

All similitude relations needed in the test are listed in Table 1.

2.3. Design of model box

Twelve rigid model boxes were fabricated and connected in line, as shown in Fig. 3. It can be seen from the figure that four model boxes which is 4 m long each are named active model boxes, while other eight whose length is 3 m each are inactive ones.

Fig. 4 shows photographs of a manufactured active model box and schematics for installation. The dimensions of each active model box are 4 m long (x), 4.5 m wide (y) and 1.2 m high (z) as shown in Fig. 4a, while dimensions of each inactive model box are the same as active box except the length. Each active model box is installed on a shaking table (Fig. 4b), while the inactive boxes stand on the manufactured steel frames, as shown in Fig. 4c. Fig. 5 shows a photograph and a schematic diagram of the steel frame. Counterbraces are placed between the frame columns for stability, and universal ball joints are fixed between inactive model boxes and support frames to eliminate friction. Frames can be vertically adjusted to make sure the inactive boxes in the same elevation as the active ones. The connection between model boxes is conducted using a hinge device and two steel connectors, as shown in Fig. 6. The hinge device, which is centered on the side of the box bottom, consists of a steel shaft and a rectangular perforated board. Each connector is placed at the bottom corners of the box and made of a piece of rebar and two steel plates welded together.

2.4. Design of model soil

Seismic response of model field is primarily a function of the small strain soil property (Assimaki, et al., 2000). The method of prototypes is therefore especially suited to this complex scale modeling problem. The length of the model field in this test is set to 40 m, and the maximum height reaches 1.1 m according to the predefined geometry similitude ratio. In addition, acceleration similitude ratio was predetermined as $Sa=5$.

As shown in Fig. 7, the fine silty sand was widely found at the site of research area (the rectangular), and the soil properties do not satisfy the similitude relation of this test as expected. Then a synthetic model soil was developed to meet the similitude relation of this test. The study of synthetic soil were introduced by other researchers, such as that of Tavenas et al. (1973) who described the development of an synthetic model soil using kaolinite, Portland cement and bentonite to replicate brittle Lake Champlain clay. Blaney and Mallow (1987) tested numerous stiffening agents used in conjunction with bentonite to fabricate a kind of synthetic overconsolidation clay for dynamic soil–pile interaction tests. Meymand (1998) mixed 67.5% kaolinite, 22.5% bentonite, and 10% class C fly ash, at 100% water content into model soil. Shang et al. (2006) designed a model soil composed of sawdust and clay for shaking table test. Dynamic tri-axial test results indicated that the unit weight and dynamic shear modulus are far below than the original clay soil.

Based on above experience, a mixture of sawdust and sand was selected as the synthetic soil for this study. A series of trial and error dynamic tri-axial tests were conducted to find the optimal mixture content of the model soil. The confining stress of the model soil in the dynamic triaxial shearing test was determined by the similitude ratio for stress S_σ and the confining stress of the field soil, which is related to the practical water pressure at the depth where the soil locates. The grain size distributions d10, d30 and d60 for the prototype soil are 0.05 mm, 0.16 mm and 0.26 mm, respectively. For the component of model soil, i.e. sand, the average diameter is 0.30 mm, and the proportion of grains with the diameter over 0.25 mm is more than 50% among all the sand. Note that the model soil was always kept in dry condition for both the triaxial test and the shaking table test.

The mixture with mass content 1:2.5 (1 for sawdust and 2.5 for sand) provided the best match with the similitude relation of Eq. (5). Table 2 lists the properties of the field soil

Table 1
Similitude relation expressions

Item	Symbol	Item	Symbol
Strain	S_ε	Velocity	$S_v = S_{Gd}^{1/2}\cdot S_\rho^{-1/2}$
Geometry	S_l	Time	$S_t = S_l\cdot S_{Gd}^{-1/2}\cdot S_\rho^{1/2}$
Unit weight	S_ρ	Frequency	$S_\omega = S_{Gd}^{1/2}\cdot S_l^{-1}\cdot S_\rho^{-1/2}$
Dynamic shearing modulus	S_{Gd}	Stress	$S_\sigma = S_{Gd}$
Mass	$S_m = S_\rho\cdot S_l^3$	Acceleration	$S_a = S_{Gd}\cdot S_l^{-1}\cdot S_\rho^{-1}$

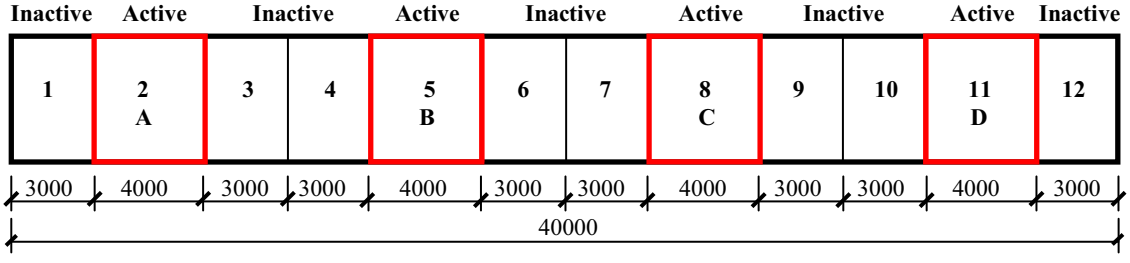

Fig. 3. Arrangement of model boxes (unit: mm).

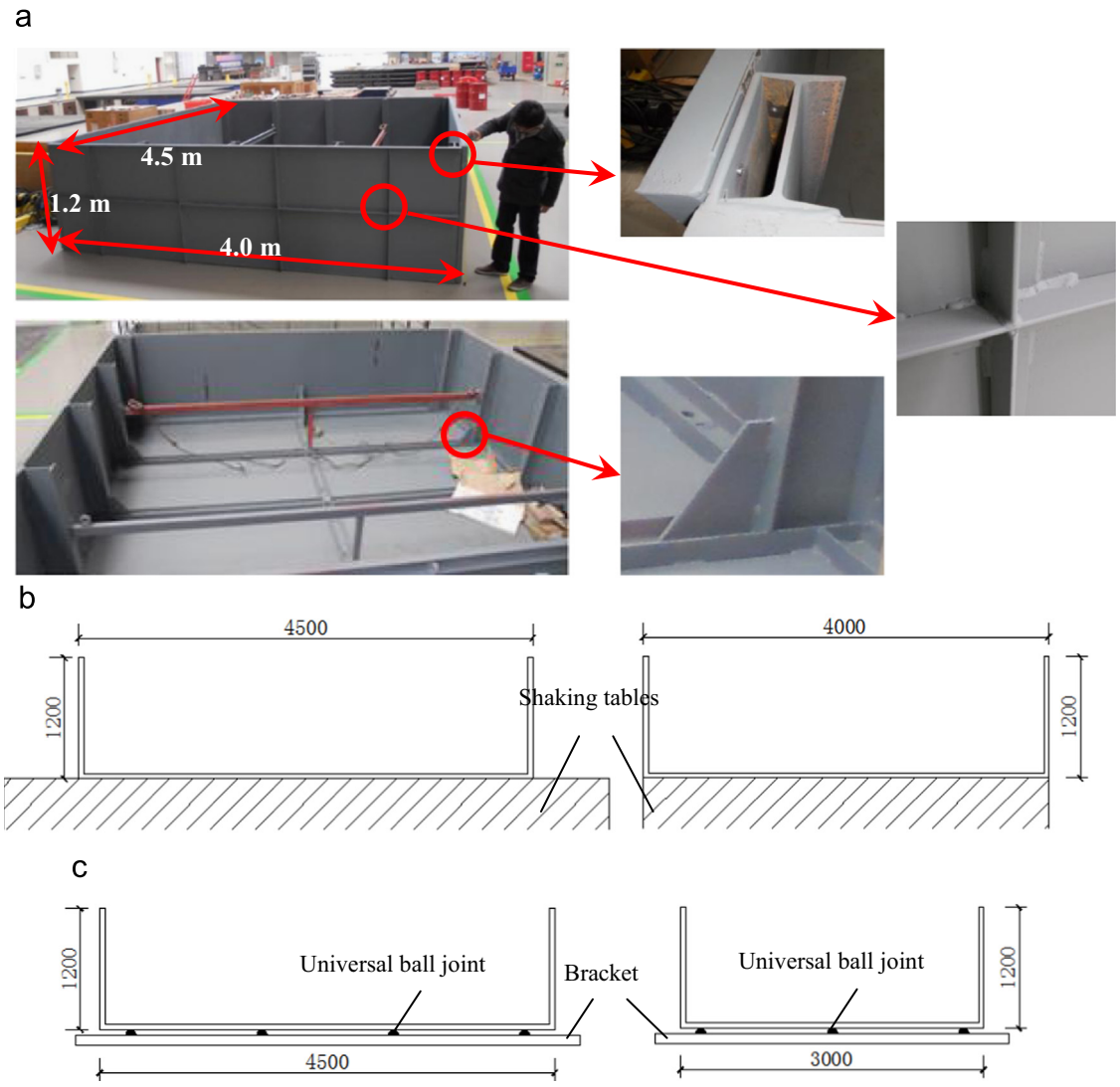

Fig. 4. The model box.

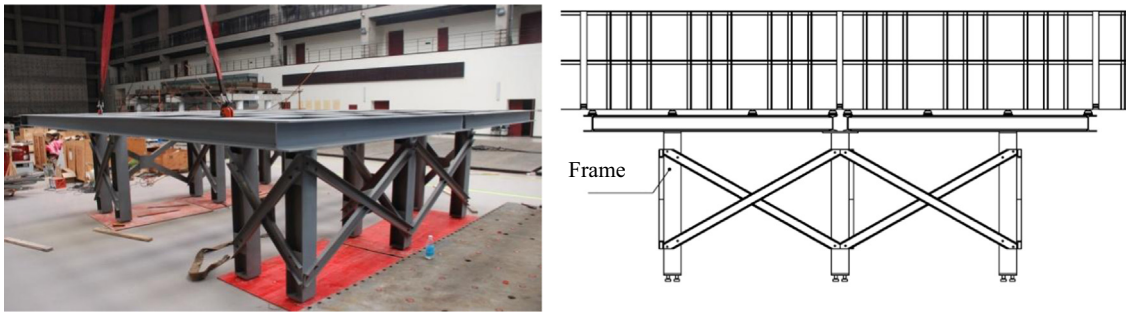

Fig. 5. The frame.

and the model soil. Fig. 8 shows the shear modulus degradation and the damping ratio increase of field soil and model soil. It can be seen that the model soil reproduces well the properties of the field soil. Finally, all similitude ratios needed in this test were obtained by the similitude equations, as listed in Table 3.

During the test, the model soil was filled into model containers layer by layer. Each layer was tamped using a block of steel with dimensions 60 cm × 60 cm × 20 cm. The steel block was lifted by a crane and placed against the surface of each layer repeatedly until final thickness of each layer was reached. This was done by placing targeted marks on the inside

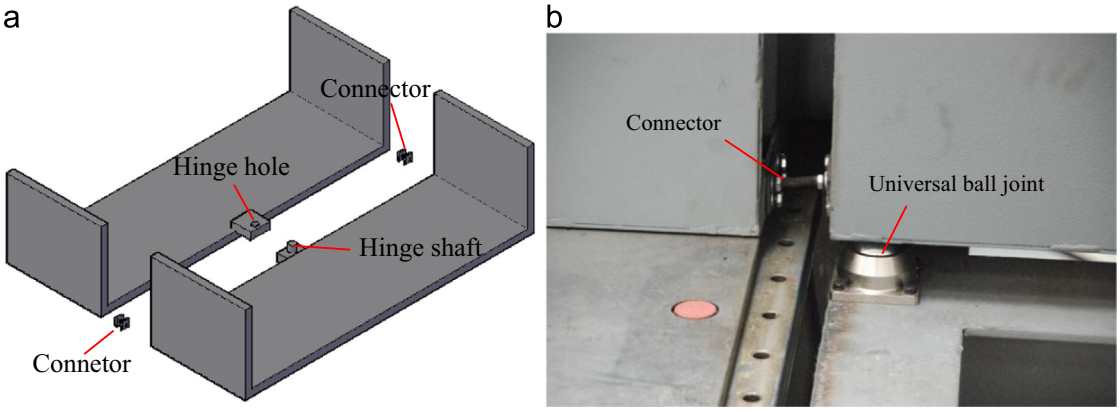

Fig. 6. The joint of model boxes, (a) hinge device and (b) connector device.

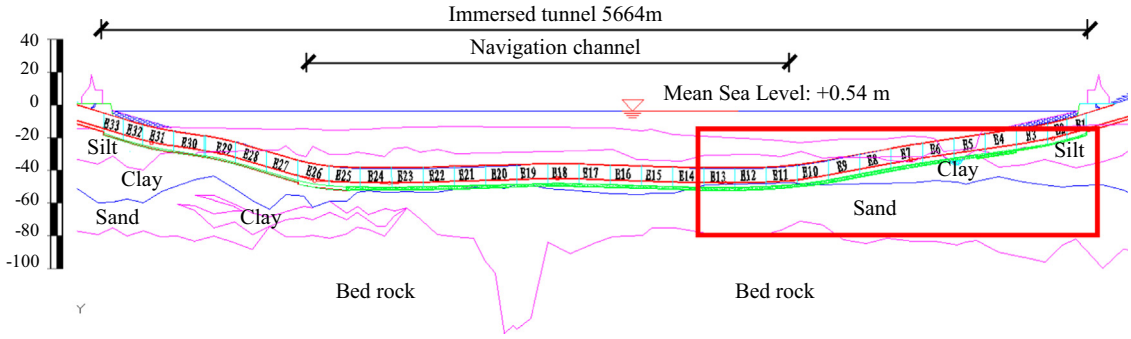

Fig. 7. Layout of immersed tunnel and ground layers (unit: m).

Table 2
Properties of field soil and model soil.

Prototype soil		Model soil		Similitude ratio	
ρ (g/cm^3)	G_d (MPa)	ρ (g/cm^3)	G_d (MPa)	S_ρ	S_{G_d}
1.67	104.5	0.694	2.84	0.416	1/37

Table 3
Similitude ratio.

	Similitude ratio		Similitude ratio
Strain	1	Velocity	0.288
Geometry	1/60	Time	0.0578
Unit weight	0.4	Frequency	17.3
Dynamic shearing modulus	1/30	Stress	1/30
Mass	1.85×10^{-6}	Acceleration	5

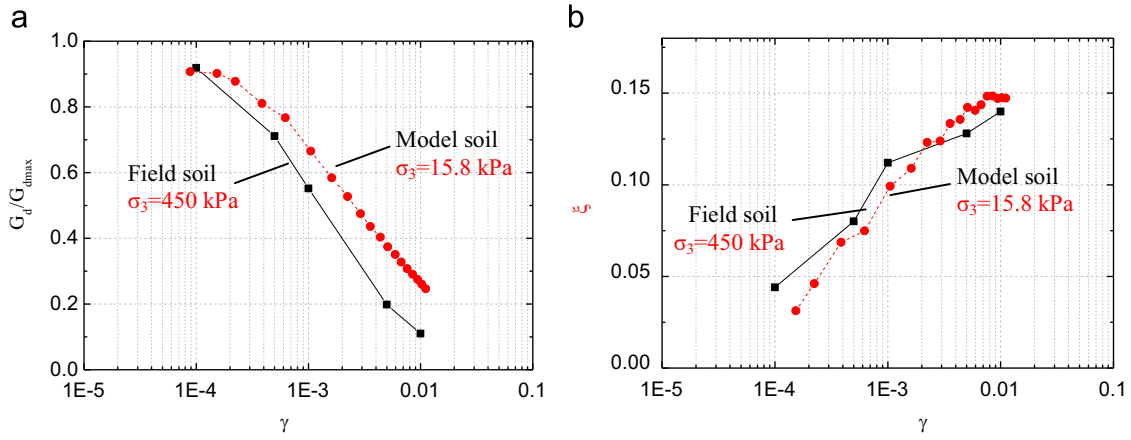

Fig. 8. Dynamic properties of model soil and prototype soil, (a) soil stiffness degradation and (b) damping.

face of the model container, and meanwhile, samples were taken and measured to make sure the soil density in each layer is consistent. Grid lines were painted on the slope surface in M1 and M12 for monitoring, as shown in Fig. 9.

2.5. Test cases

The experiments were conducted in two phases with a total 38 test cases. All twelve model boxes were used in Phase 1 and were kept empty since the objective was to investigate the performance of the soil containers and check the multi-point input mechanism. Phase 2 is the model field test to investigate seismic response of model soil under non-uniform seismic loadings. Test cases are summarized in Table 4, and different input parameters are considered including seismic wave, vibration direction, peak acceleration and wave propagation direction.

2.6. Instrumentation

A number of unidirectional accelerometers were adopted to record the seismic response during the tests. Fig. 10 shows the sensor location. Arrangement of sensors is different for each test phase due to the test objectives. The following terminology is used to describe the sensors: M stands for model box, while X and Y are longitudinal and transversal direction, respectively. Fig. 10a shows plan view of the layout of accelerometers in test phase 1: two accelerometers were installed at the center of bottom board in each box. Total 76 accelerometers were embedded in the soil in test phase 2. Fig. 10b, c and d shows the three orthographic views of the layout of accelerometers in test phase 2, i.e. plan view, side view and cross-section view, respectively.

3. Model box test result and discussion

3.1. Input mechanism

Twelve rigid model boxes are connected in line along the longitudinal direction using a flexible joint between each adjacent model box, in order to investigate the wave passage effect along the length of the connected model boxes. The total length of this test is 40 m, which is much larger than the excitation zone (16 m). Then, a discrete multi-point non-uniform input scheme is necessary to simulate the wave passage effect along the four shaking tables. The objective of model box test without soil (i.e. Phase 1) is to check the design of the system of shaking table tests, more specifically, to realize the transformation from multi-point discrete input mechanism into continuous mode via the design of the model box, as envisioned. To realize that, the principle of equivalence between discrete and continuous excitations should be satisfied as follows: (1) the maximum response acceleration of inactive boxes should basically be equal to that of active boxes; (2) the main frequency of inactive boxes should be coincidence with that of active boxes under; and (3) time delays at the active and inactive boxes should be clearly observed along the wave passage direction.

To simulate the wave passage effect along each of the four shaking tables, a time lag Δt is imposed to the motion of each table. It is given by:

$$\Delta t = l_i / C_\alpha$$

where l_i is the distance between two shaking tables, and C_α is the wave velocity at the bedrock. A harmonic wave with peak acceleration 0.25 g, was selected to input in the non-uniform

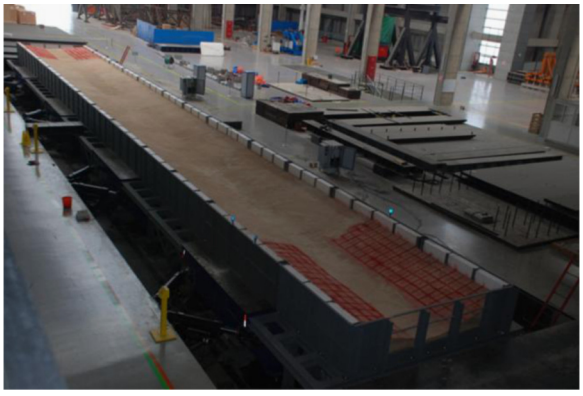

Fig. 9. The prepared model field.

Table 4
Test cases.

Test case	Input wave form	Vibration direction	Peak acceleration	Excitation form
Phase 1: model box test				
K1-K2	Harmonic	Longitudinal/transversal	0.25 g	Non-uniform (A to D)
Phase 2: free field test				
Z1-Z36	Synthetic/El Centro/Kobe	Longitudinal/transversal	0.25 g/0.75 g	Uniform/non-uniform (A to D/D to A)

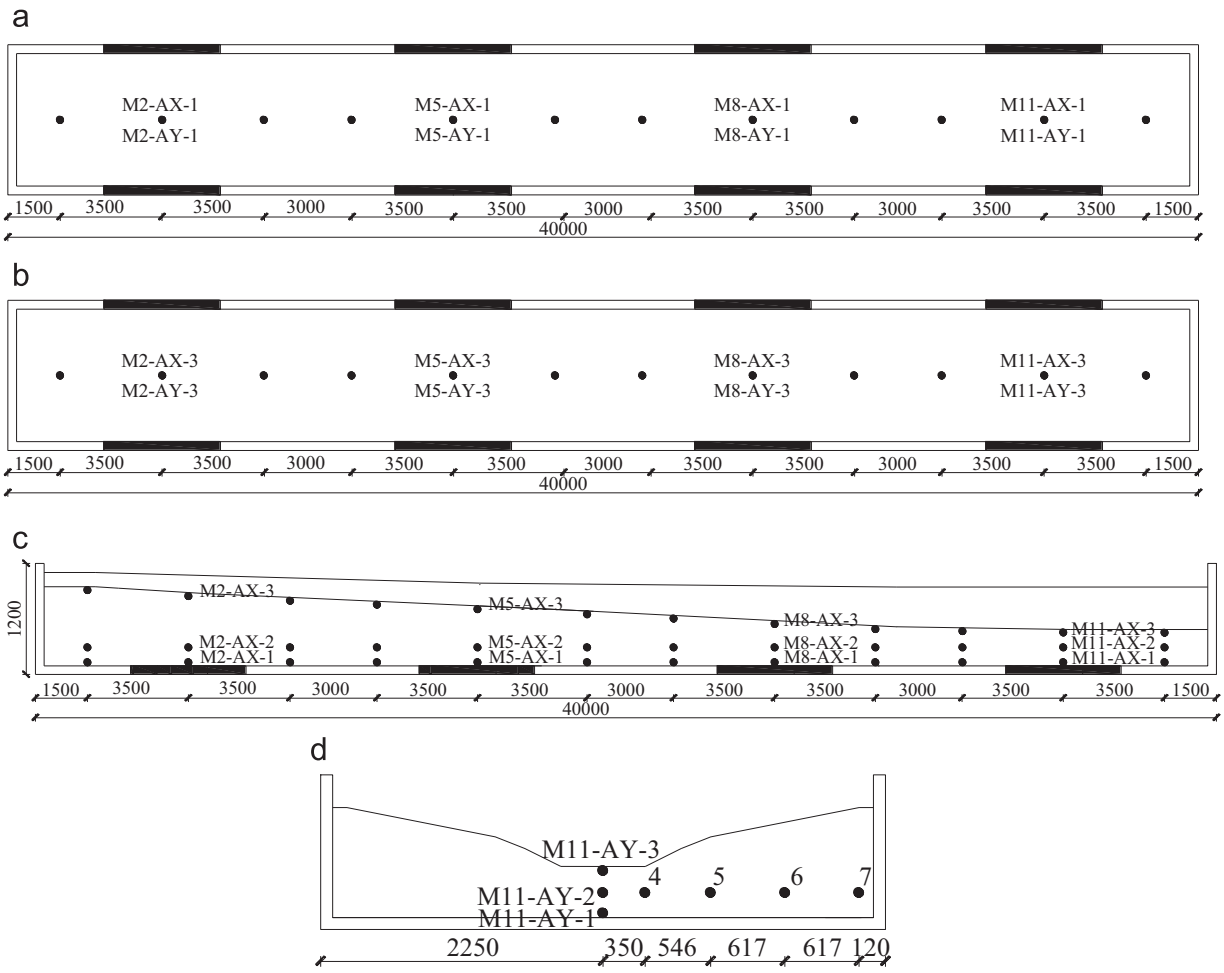

Fig. 10. Instrumentation for test (unit: mm), (a) layout sensors in Phase 1 test, (b) layout sensors in Phase 2 test, (c) side view in Phase 2 test, and (d) cross-section view in model box M11.

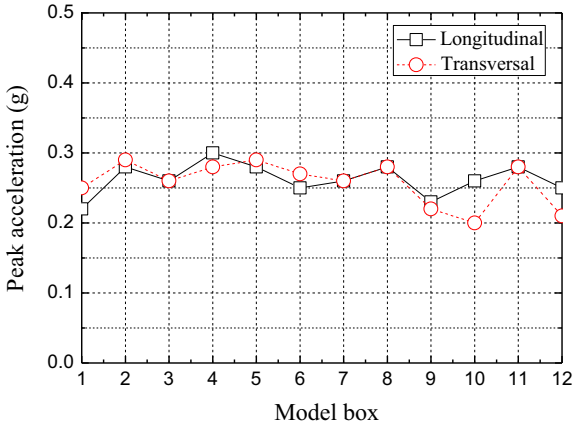

Fig. 11. Peak acceleration response in model boxes.

style, and the wave frequency was 50 Hz. Assuming the prototype apparent wave velocity is 1000 m/s, the test wave velocity will be 288 m/s according to similitude ratio for velocity $S_v = 0.288$. The distance between the centers of any two adjacent shaking tables is 10 m, therefore the time lag of wave propagation is about 0.035 s. Shaking tables worked as a sequence D, C, B and A. Two independent tests were run: the first one was in longitudinal direction, and the second in transversal direction.

3.2. Acceleration response

It is necessary to compare the actual acceleration responses of active model boxes with that developed in inactive model boxes.

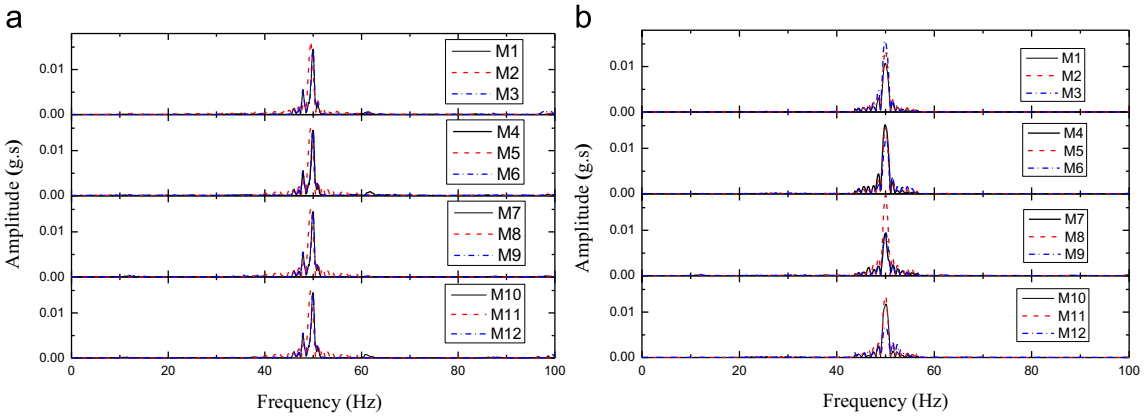

Fig. 12. Spectra of acceleration response, (a) KS1 case (longitudinal excitation) and (b) KS2 case (transversal excitation).

Table 5
Phase of model boxes (unit: in deg)

Model box	1	2	3	4	5	6	7	8	9	10	11	12
KS1	−80	68	−76	138	−25	−170	49	−114	88	−74	158	10
Difference	−212	216	214	197	215	219	197	202	198	232	212	
KS2	65	−122	78	−61	139	−13	−158	58	−104	96	−42	179
Difference	−187	200	221	200	208	215	216	198	200	222	221	

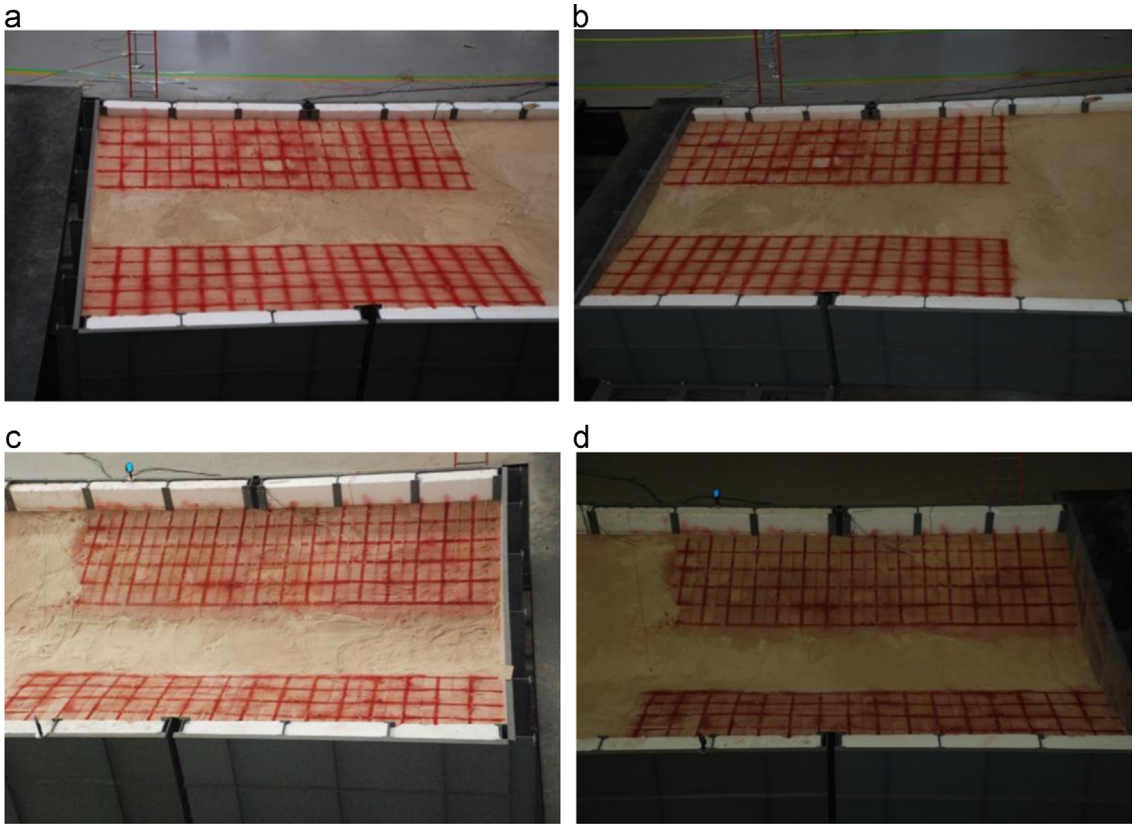

Fig. 13. Grid lines on slope surface, (a) model box No.1 before test, (b) model box No.1 after test, (c) model box No.1 before test, and (d) model box No.1 after test.

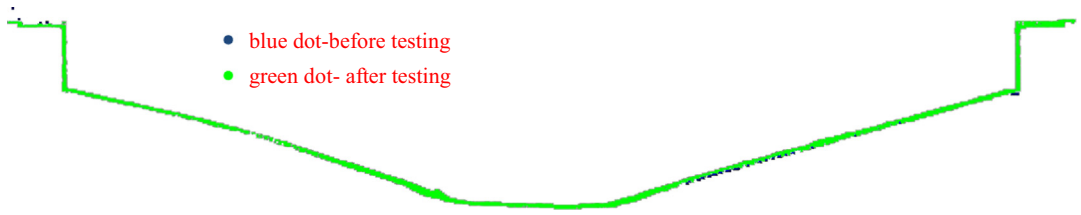

Fig. 14. Outlines of slope before and after test. (For interpretation of the references to color in this figure, the reader is referred to the web version of this article.)

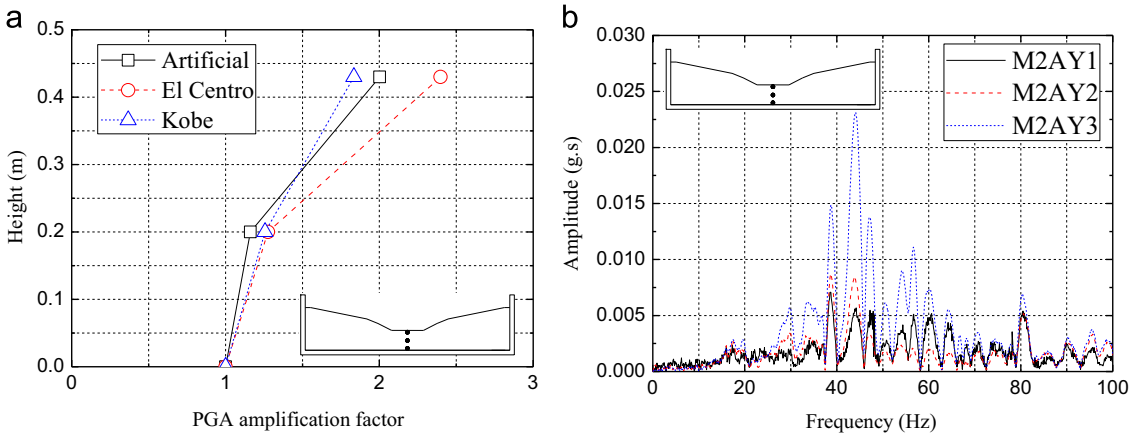

Fig. 15. The acceleration response along vertical direction (excitation in transversal direction), (a) acceleration amplification factor and (b) spectrum of acceleration.

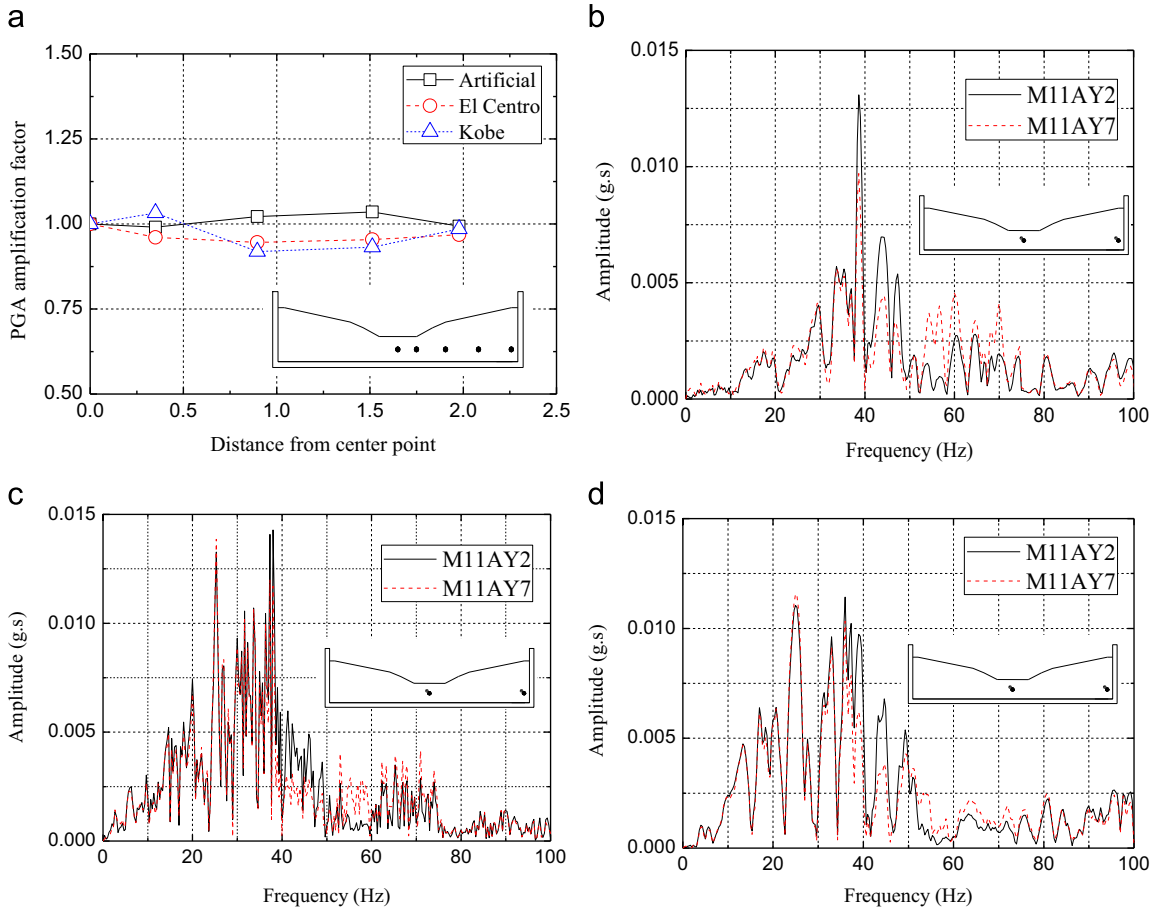

Fig. 16. Comparison of acceleration response for evaluating boundary effect, (a) PGA amplification factor, (b) synthetic wave, (c) El Centro wave, and (d) Kobe wave.

Fig. 11 provides the peak acceleration at each model box. As can be seen in the figure, the responses in active model boxes are 0.28 to 0.29 g, while the responses in inactive model boxes ranged from 0.2 g to 0.3 g. Thus, it is acceptable that peak accelerations in inactive box are basically consistent with that in active boxes.

3.3. Fundamental frequency

Spectra analysis is performed on time histories of all sensors in test case KS1 and KS2. Fig. 12 shows the acceleration spectra of all active and inactive boxes. It is found that the fundamental frequencies of all active and inactive boxes are the same 50 Hz for both longitudinal and transverse excitation.

3.4. Phase difference

Phase difference is usually used in investigating wave passage effect appeared in soil field (21-23). In this test, time lag between any two adjacent active model boxes is about 0.035 s as previous stated. Then phase difference φ can be calculated as

$$\varphi = \omega\Delta t = 2\pi f \Delta t$$

where the fundamental frequency $f = 50$ Hz, then the phase difference $\varphi = 630^\circ$. Table 5 lists the phase difference registered at each box. It can be found that phase differences between adjacent active model boxes are basically consistent with the target value, and the difference between connected boxes ranged 187–222°, which is close and deemed acceptable.

Based on test results, peak accelerations and fundamental frequencies of active model boxes are consistent with those observed on inactive model boxes. This is also the case for the phase difference. Thus, the wave passage effect is reproduced, and the design of the multi-point input scheme is adequate.

Table 6
Standard test cases.

Test case	Seismic wave	Vibration direction	Peak acceleration	Excitation form
Z1	Synthetic	Y	0.25 g	Non-uniform (A to D)
Z2	Synthetic	X	0.25 g	Non-uniform (A to D)

4. Model ground test result and discussion

4.1. General observation

As previous stated, grid lines have been drawn on surface of the slope at the end in model box M1 and the critical area in model box M12 as shown in Fig. 13a and c. Fig. 13b and c displays the model field in M1 and M12 after all the tests were completed, respectively. It is found that mesh distortion on the slopes can hardly be seen in both boxes.

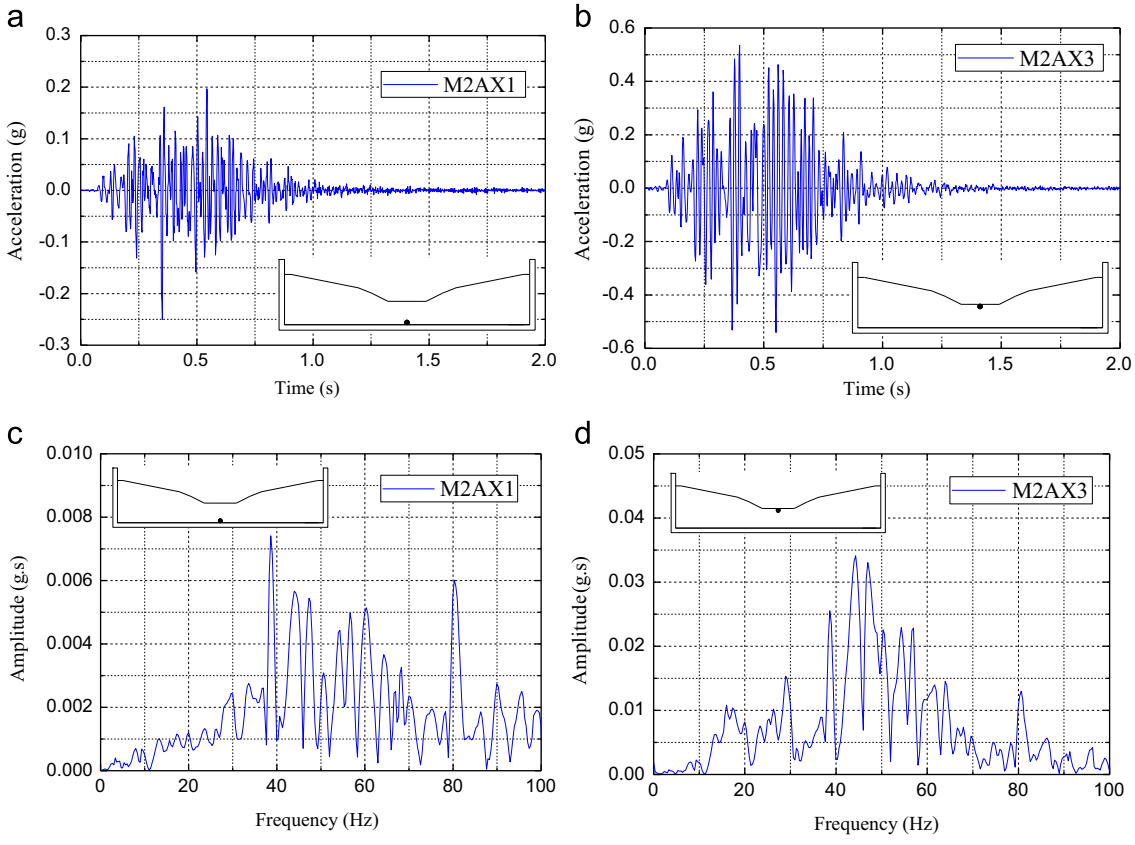

Fig. 17. Acceleration response for vibration in longitude direction, (a) acceleration time history for M2AX1, (b) acceleration time history for M2AX3, (c) acceleration spectrum for M2AX1, and (d) acceleration spectrum for M2AX3.

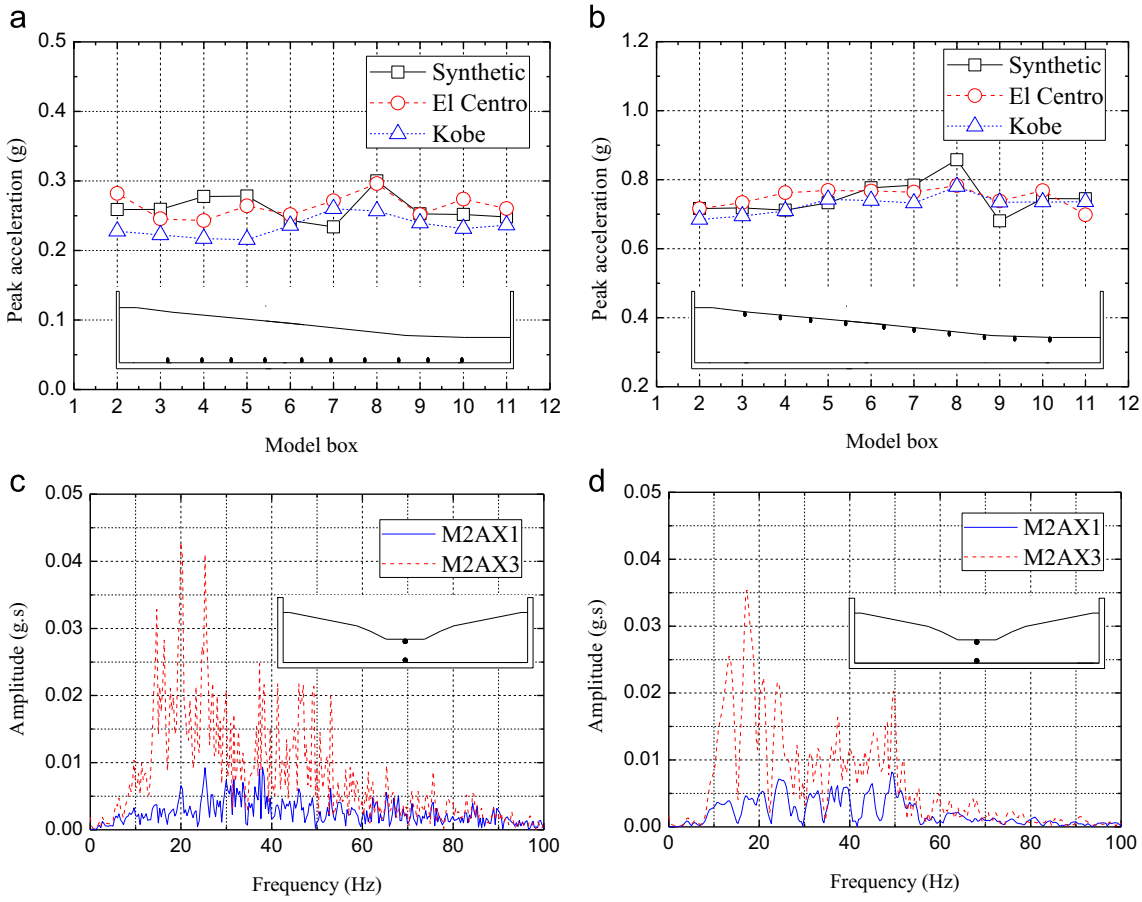

Fig. 18. Comparison of acceleration response under different sort of waves, (a) peak accelertion for bottom of model field, (b) peak acceleration for top of model field, (c) acceleration spectra for El Centro wave case, and (d) acceleration spectra for Kobe wave case.

A laser scanner device was utilized to observe field cross section in model box M11. Fig. 14 shows outlines of slope before and after test, in which the blue dots represent outline of slope before test and green dots represent that after test. It can be found that the two outlines are basically overlapped, which is indicative of small deformations in the soil under seismic loadings.

4.2. Amplification factor and boundary effect

Fig. 15 shows the acceleration response along vertical direction. For comparison purposes, the peak acceleration recorded by sensors M2AY2 and M2AY3 are normalized by the peak value of M2AY1. Results from the Fig. 15a indicate that, amplification factors imply magnification trend along vertical direction. Fig. 15b shows the acceleration spectra from the three observation points, and the amplification trend can also be found along vertical direction.

Boundary effect of soil container is unavoidable in shaking table tests of model field. It is introduced that energy absorption material was used on boundary of rigid model boxes (Moss and Crosariol, 2013; Lombardi, et al., 2015). In this test, a number of 200-mm-thick polystyrene foam boards were stuck to inner sidewalls of all twelve model boxes. Five accelerometers were embedded at the same elevation in model box M11 to record seismic response in transversal direction. For comparison purpose, peak acceleration recorded by sensors M11AY4, M11AY5, M11AY6 and M11AY7 are normalized by that of M11AY2. Fig. 16 shows the acceleration responses from the five sensors. It can be observed from Fig. 16a that the PGA amplification factors are close at these points. Fig. 16b, c and d display comparisons of acceleration spectra at M11AY7, near the boundary and M11AY2, at the center. Test results indicate that the seismic responses of the two points are similar, thus boundary effect in this test is negligible.

4.3. 4.3 Test standard condition

It is critical to investigate the seismic response of model field in different input methods in this test. For this purpose, it is necessary to select typical test cases as standard. Two test cases were selected as shown in Table 6. Fig. 17 shows acceleration response under longitudinal excitation recorded by sensors M2AX1 and M2AX3, which locate at bottom and top of model field in model box M2. Acceleration time histories of M2AX1 and M2AX3 are shown in Fig. 17a and b, while acceleration spectra are shown in Fig. 17c and d. Comparing

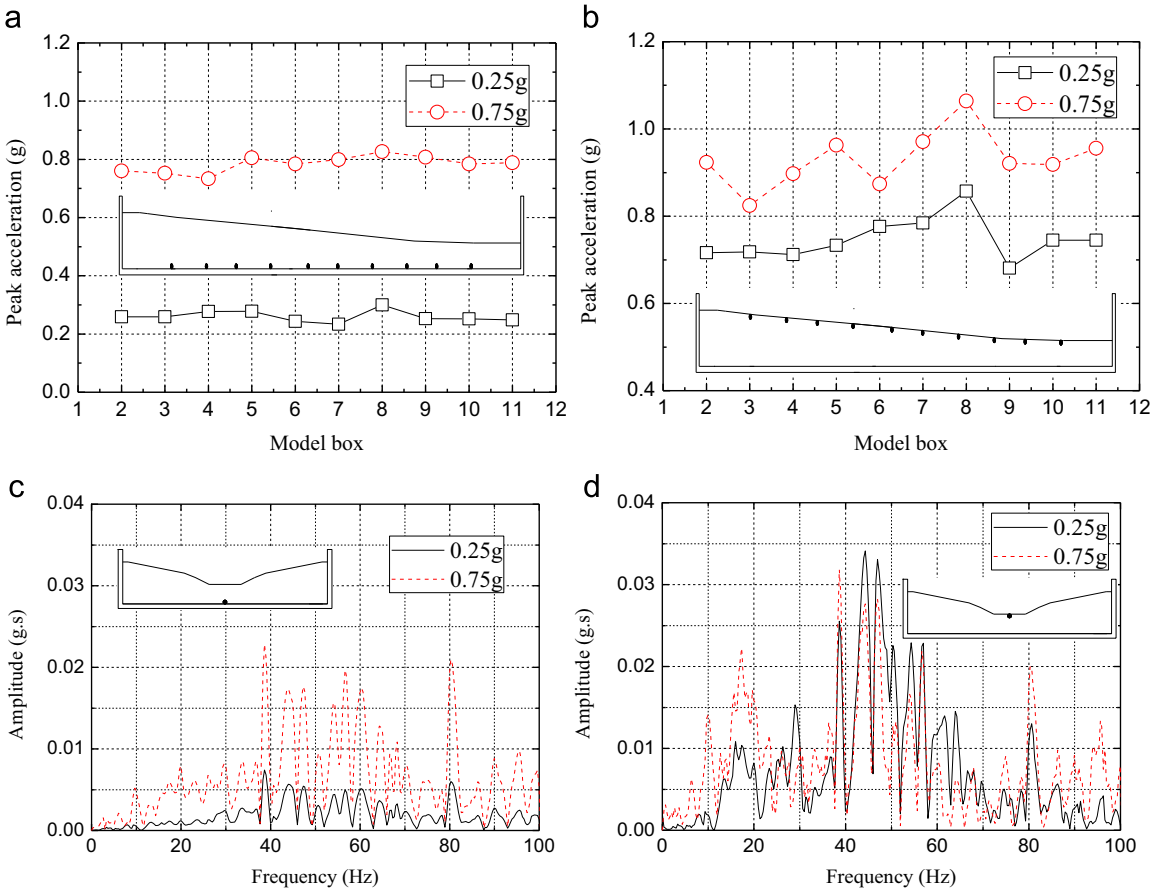

Fig. 19. Comparison of acceleration response for different excitation magnitude, (a) peak acceleration for bottom of the model field, (b) peak acceleration for top of the model field, (c) acceleration spectra for M2AX1, and (d) acceleration spectra for M2AX3.

the seismic responses at bottom and top of the model field, it can be seen that the wave is not linear scaled in vertical direction and may be effected by the soil. Similar phenomenon was observed in other model boxes.

4.4. Seismic wave form

Three sort of seismic waves, i.e. the synthetic wave, El Centro wave and Kobe wave, were input to investigate responses of model field, respectively. Fig. 18a and b shows the peak acceleration at bottom and top of the model field, while Fig. 18c and d displays the spectra in El Centro and Kobe cases (the corresponding spectra in synthetic case are show in Fig. 17c and d). The peak acceleration in each box was observed to be close at same monitoring point in all three cases. However, model field performed unlikely in the frequency domain, and the spectra show different waveforms under the three sort of seismic loadings.

4.5. Peak acceleration

Different input magnitude of seismic waves was evaluated in the shaking table tests. Synthetic waves with peak acceleration 0.25 g and 0.75 g were input to investigate seismic response of the model field, respectively. Fig. 19a and b shows the response peak acceleration at bottom and top of the model field, and Fig. 19c and d depicts the acceleration spectra for M2AX1 and M2AX3 under different excitations. The first two figures indicate that the peak accelerations at the top are 2.5–3.4 times amplified from the bottom responses in 0.25 g case, however the corresponding amplification factor is only 1.1–1.3 in 0.75 g case. As shown in Fig. 19c and d, the spectra for the two cases are similar in shape, but different in amplitude. It can be concluded that the model soil does not linearly amplify the seismic response in vertical direction.

4.6. Vibration direction

Dynamic responses of the model field were investigated in the conditions excited seismic loadings in transversal direction and in longitudinal direction. Fig. 20 shows peak acceleration and spectra for excitation in longitudinal direction and in transversal direction. It is clearly observed that seismic responses caused by loadings in longitudinal direction are close to those in transversal direction. Comparatively, however, responses at the surface of the model field under longitudinal excitation were observed larger than those under transversal excitation at several observation points.

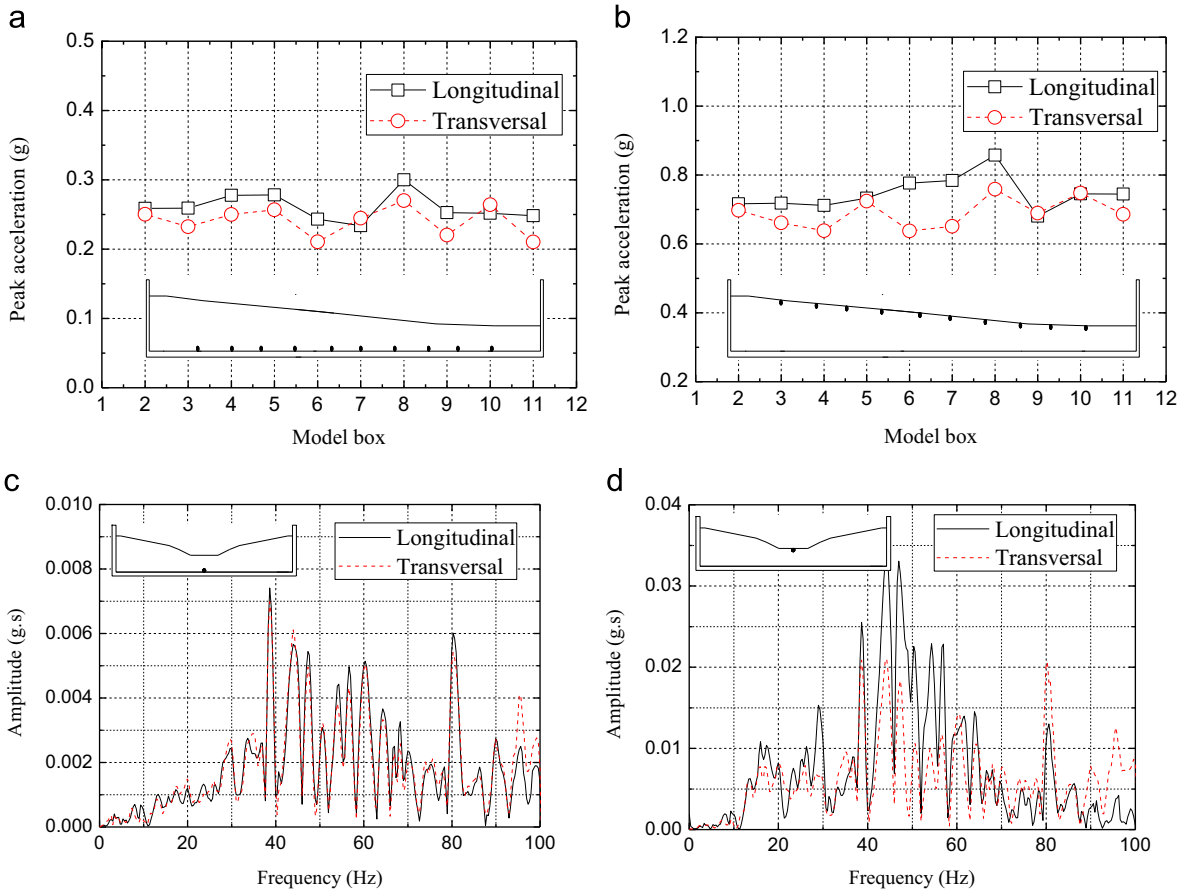

Fig. 20. Comparison of acceleration responses for different excitation direction, (a) peak acceleration at bottom of the model field, (b) peak acceleration at top of the model field, (c) acceleration spectra for M2AX1, and (d) acceleration spectra for M2AX3.

4.7. Excitation sequence

Typically, the excitation sequence is shaking table A works first, then B, then C, and at last D. In this test, however, seismic response of the model field is also estimated in reverse input sequence. Fig. 21 shows the comparison of acceleration responses under two different excitation sequences, i.e. from A to D and from D to A. Test results show that model soils at the same observation point perform similarly under the two sequences. Note that the maximum slope angle along the longitudinal direction is no more than 1° and thus has a negligible effect on the seismic responses of the model soil.

5. Conclusion

The work of this paper presents the results of the seismic response of the submerged portion of the Hong Kong–Zhuhai–Macau Bridge. A 40-m-long shaking table test was designed and carried out using four shaking tables in the laboratory. Detailed information for design of the similitude relation, the long model boxes and the synthetic soil, have been described and should be useful for further similar tests. Performance of the model box has been checked by the shaking table tests using twelve connected boxes without soil. The results showed that the wave passage effect is accurately reproduced with the test setup and the non-uniform input scheme. A series of shaking table tests were conducted to investigate the performance of the model field, under non-uniform earthquake wave excitation. Several factors for excitation were evaluated, including sort of waves, magnitude of earthquake, excitation direction and input sequence. Test results demonstrated that the seismic waves could be amplified in vertical direction, and boundary effect was negligible and did not affect the response of the synthetic soil in the model box. Model field does not show linear amplification behavior in vertical direction, under earthquake of different magnitude. Acceleration responses under longitudinal excitation are close to those under transversal excitation, except several points at top surface of the model field. Model soils at the same observation points perform similarly under the two different excitation sequences, due to the negligible difference of the field slope along the longitudinal direction.

Additional research focuses on the interaction of the tunnel model and the model field. However, the result is beyond the scope of this paper and will be the focus of a future publication.

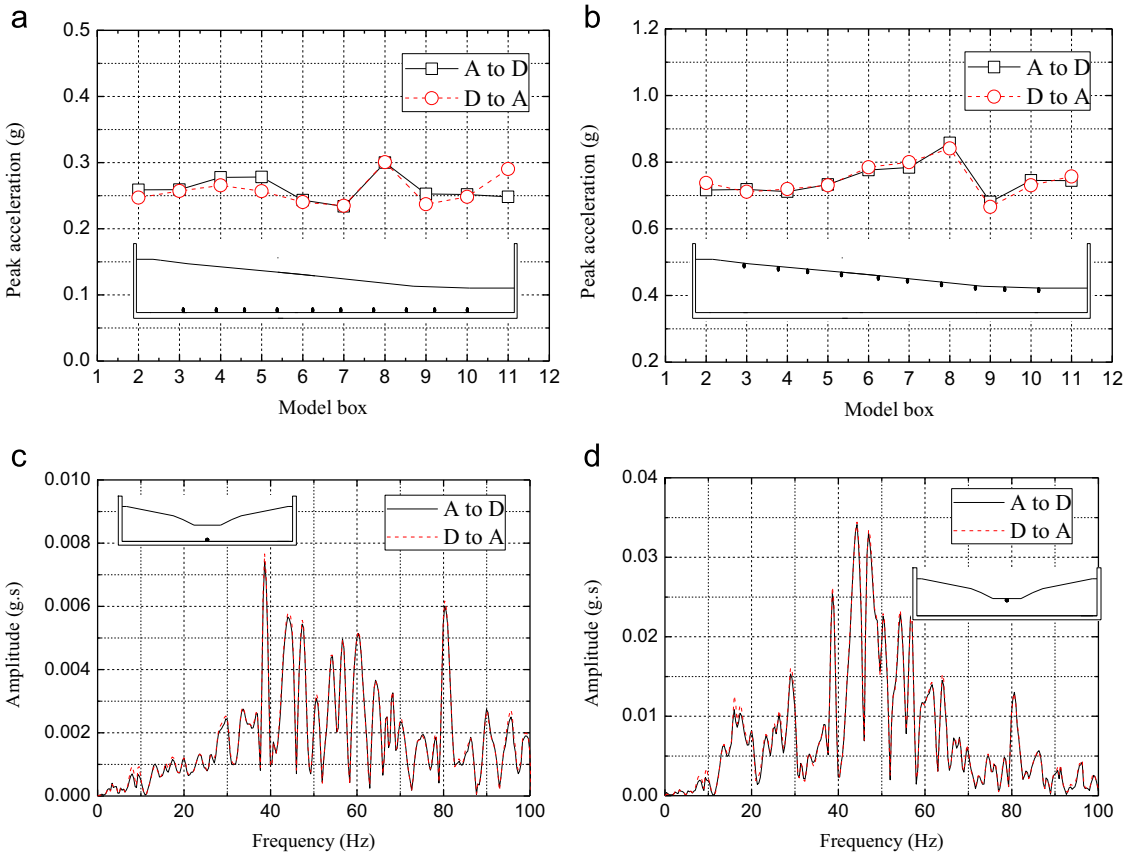

Fig. 21. Comparison of acceleration responses under different input sequence, (a) peak acceleration for bottom of the model field, (b) peak acceleration for top of the model field, (c) acceleration spectra for M2AX1, and (d) acceleration spectra for M2AX3.

Acknowledgments

The research has been supported by the National Natural Science Foundation of China, China (51208296 and 51478343) and the Shanghai Committee of Science and Technology, China (13231200503). The authors acknowledge the support from the Fundamental Research Funds for the Central Universities, China, Shanghai Educational Development Foundation, China (13CG17), and the National Key Technology R&D Program, China (2012BAK24B04).

References

Assimaki, D., Kausel, E., Whittle, A., 2000. Model for dynamic shear modulus and damping for granular soils. J. Geotechn. Geoenviron. Eng. 126 (10), 859–869.

Blaney, G., Mallow, W., Synthetic clay soil for dynamic model pile tests. Proc., Dynamic Response of Pile Foundations-Experiment, Analysis, and Observation, Geotech. Spec. Pub. 11, T. Nogami, ed., ASCE,Reston, Va., 127-148.

Brennan, A., Thusyanthan, N., Madabhushi, S., 2005. Evaluation of shear modulus and damping in dynamic centrifuge tests. J. Geotechn. Geoenviron. Eng. 131 (12), 1488–1497.

Chen, J., Shi, X., Li, J., 2010. Shaking table test of utility tunnel under non-uniform earthquake wave excitation. Soil Dyn. Earthq. Eng. 30 (11), 1400–1416.

Fang, L., Chen, J., Cao, H., Mo, H., Liu, S., 2011. Study on stability of underwater trench of immersed tunnel of Hongkong–Zhuhai–Macau Bridge. Appl. Mech. Mater. 90-93, 2212–2220.

Gazetas, G., 1987. Seismic response of earth dams: some recent develops. Soil Dyn. Earthq. Eng. 6 (1), 2–47.

Hashash, Y., Hook, J., Schmidt, B., Yao, J., 2001. Seismic design and analysis of underground structures. Tunn. Undergr. Sp. Technol. 16, 247–293.

Hong, Y., Chen, R., Wu, C., 2005. Shaking table tests and stability analysis of steep nailed slopes. Can. Geotech. J. 42 (5), 1264–1279.

Huang, C., Horng, J., Chang, W., Chiou, J., Chen, C., 2011. Dynamic behavior of reinforced walls-horizontal displacement response. Geotext. Geomembr. 29 (3), 257–267.

Iai, S., 1989. Similitude for shaking table tests on soil-structure-fluid model in 1 g gravitational field. Soils Found. 29 (1), 105–118.

Iwasaki, T., Tatsuoka, F., Takagi, Y., 1978. Shear moduli of sands under cyclic torsional shear loading. Soils Found. 18 (1), 39–56.

Kasper, T., Steenfelt, J., Pedersen, L., Jackson, P., Heijmans, R., 2008. Stability of an immersed tunnel in offshore conditions under deep water wave impact. Coast. Eng. 55 (9), 753–760.

Kutter, B., 1983. Deformation of centrifuge models of clay embankments due to 'bumpy road' earthquakes. Soil Dyn. Earthq. Eng. 2 (4), 199–205.

Lin, M., Wang, K., 2006. Seismic slope behavior in a large-scale shaking table model test. Eng. Geol. 86, 118–133.

Ling, H., Leshchinsky, D., Mohri, Y., 1997. Soil slopes under combined horizontal and vertical seismic accelerations. Earthq. Eng. Struct. Dyn. 26. (12)1231–1241.

Lo Grasso, A., Maugeri, M., Recalcati, P., 2004. Shaking table tests and analysis of reinforced slopes. 3d Asian Regional Conference on Geosynthetics, Seoul, Korea.

Lombardi, D., Bhattacharya, S., Scarpa, F., Bianchi, M., 2015. Dynamic response of a geotechnical rigid model container with absorbing boundaries. Soil Dyn. Earthq. Eng. 69, 46–56.

Meymand, P., 1998. Soil-pile-superstructure interaction in soft clay, Ph.D. dissertation. University of California, Berkeley.

Moss, R., Crosariol, V., 2013. Scale model shake table testing of an underground tunnel cross section in soft clay. Earthq. Spectra 29 (4), 1413–1440.

Newmark, N., 1965. Effects of earthquake on dams and embankments. Geotechnique 15 (2), 139–160.

Shang, S., Liu, F., Lu, H., Du, Y., 2006. Design and experimental study of a model soil used for shaking table test. Earthq. Eng. Eng. Vib. 26 (4), 199–204.

Tavenas, F., Roy, M., La Rochelle, P., 1973. An artificial material for simulating champlain clays. Can. Geotech. J. 10 (3), 489–503.